Please cite this paper as: N. Singh, J. T. Horwood, and A. B. Poore, "Space object maneuver detection via a joint optimal control and multiple hypothesis tracking approach," in Proceedings of the 22nd AAS/AIAA Space Flight Mechanics Meeting, Charleston, SC, January 2012 (Paper AAS-12-159)

AAS 12-159

SPACE OBJECT MANEUVER DETECTION VIA A JOINT OPTIMAL CONTROL AND MULTIPLE HYPOTHESIS TRACKING APPROACH

Navraj Singh, Joshua T. Horwood, and Aubrey B. Poore*

An optimal control framework is presented as a post-processor to a multiple hypothesis tracker for resolving uncorrelated tracks (UCTs) generated by space object maneuvers. The optimal control framework uses the total velocity increment ΔV as the cost functional to determine feasibility of maneuvers. The method obtains accurate ΔV estimates for connecting two UCTs via fuel-optimal maneuvers. In addition, a method is proposed for treating uncertainty in the UCT states, via the unscented transform, to determine the probability that a maneuver is feasible. The approach is most applicable to routine but unannounced fuel-optimal maneuvers conducted by space objects.

INTRODUCTION

A critical requirement in achieving robust space situational awareness (SSA) is the ability to process and reduce the number of uncorrelated tracks (UCTs), which are newly acquired tracks on objects that do not associate (correlate) with any known objects in the space catalog.[1] While there are many reasons for UCTs, a common source is that of a maneuvering space object. The ability to assess the possibility of maneuvers from UCT observations is therefore an important goal in SSA. Our approach to this problem, presented in this paper, is to first use a modern tracking system such as a multiple hypothesis tracker (MHT)[2] to detect broken tracks and UCTs. If an object is not seen within a predicted gate and subsequently a UCT is generated by it, then we propose an optimal control framework, as a post-processor, for maneuver detection and track stitching. This work has its origin in the recent work of Holzinger and Scheeres.[3] In this paper, we extend this work by first using a MHT to detect the possibility of a maneuver and then using an optimal control framework based on the ΔV cost functional (which is directly proportional to fuel-cost) as a post-processor to determine the feasibility of possible maneuvers. The method is most applicable to unannounced fuel-optimal maneuvers routinely conducted by space objects for tasks such as orbit maintenance and station-keeping.

A common approach for maneuver detection in *data-rich* tracking environments (such as air and missile defense) is the dynamic multiple model framework, and in particular, the interacting multiple model (IMM) filter or the related generalized pseudo-Bayesian (GPB) filter.[4] Typically, the motion models differ in terms of their process noise parameter. The changes in the modal probabilities in an IMM (or GPB) filter can imply the possibility of a maneuver, as suggested in an AGI white paper.[5] However, in the *data-starved* space surveillance environment, maneuvers are rarely observed while they are being conducted, or they are so slow (as in a slow-burn case) that one might miss them. While a multiple model filter can still crudely detect possible maneuvers, covariance

*Numerica Corporation, 4850 Hahns Peak Drive, Suite 200, Loveland, CO 80538

consistency, which is critical for robust tracking, need not be maintained, especially if the maneuver filter model does not match the true dynamics of the maneuver. In addition, little information is obtained regarding the maneuver cost or the maneuver profile. We recommend instead an optimal control based approach for improved accuracy and for "stitching" disparate tracks linked by a maneuver.

The proposed optimal control approach is part of a broader proposal consisting of three steps: (i) detect candidate anomalies (broken tracks and UCTs) by running a MHT that does not contain any maneuvering model hypotheses; (ii) as a post-processor, use a cheap maneuver detection algorithm, such as a high process noise filter model to rule out any obvious infeasible/unlikely maneuvers; and (iii) use the optimal control framework presented in this paper for fine maneuver detection, maneuver reconstruction, and track stitching/fusion.

This paper focuses on Step (iii). The main goal of the optimal control computation step is to accurately reconstruct possible maneuvers from given track states or measurements. To achieve this, we use a framework that employs the total velocity increment ΔV as the cost functional to determine feasible maneuvers. We choose ΔV as the cost because it is directly proportional to fuel cost and, as such, it is the most important cost metric used in space object mechanics.[6] In addition, ΔV values are often catalogued in the form of ΔV budgets for many space object missions and maneuver types. Obtaining accurate ΔV estimates and associated control profiles that connect broken tracks facilitates the use of known ΔV budgets in determining feasibility of maneuvers. Although the use of ΔV in the optimal control problem leads to numerical singularities and has led others to consider alternative cost functionals, *we have overcome these numerical difficulties*. Specifically, we apply the Huber approximation[7] to make the control problem tractable. A key finding from our numerical simulations is that by using ΔV as the cost to be minimized, optimal controls are found to be impulsive in nature (disregarding spacecraft specific thrust models), which confirms known theoretical results in special cases.[8] Our results also suggest that the obtained optimal control profiles can aid in reconstructing the type of maneuver.

Finally, the end goal we seek is to obtain a reasonable estimate for the "probability of a maneuver" for a given UCT pair, and accurate ΔV estimates will be an important component of a model for this maneuver probability. In the absence of any data other than UCT track states, and under the assumption that space objects will most often conduct any maneuvers in a fuel-optimal manner, we propose to resolve possible UCT pairings according to their feasibility in terms of fuel cost of a possible maneuver linking the pair. To robustly use the obtained ΔV estimates for connecting mean UCT states, we show how to address the uncertainty in the track states that form the boundary conditions of the control problem. In particular, we describe an efficient method based on the unscented transform[9] to approximate the probability distribution of the ΔV cost. We then define a hypothesis test that determines the probability that the ΔV cost is feasible. This probability may subjectively be understood as the "probability of a maneuver." We show that a correct computation of the ΔV distribution is critical for achieving the correct UCT association. We demonstrate the general theory with several examples and show that the entire framework is robust, reconstructs accurate ΔV estimates and associated ΔV-optimal control profiles, and is an efficient method for maneuver validation and UCT resolution.

The paper is organized as follows. First, we briefly present the problem statement. Then, the optimal control problem and the method to solve it are discussed. Next, a method to treat the uncertainty in the boundary conditions of the optimal control problem is presented. Finally, simulation studies are conducted, the results are analyzed, and conclusions are made.

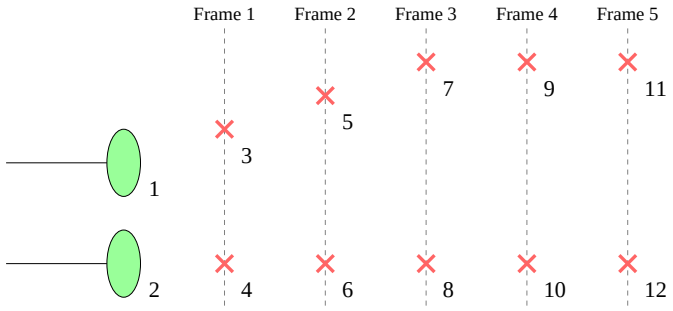

Figure 1. The data available to the MHT through the first five frames.

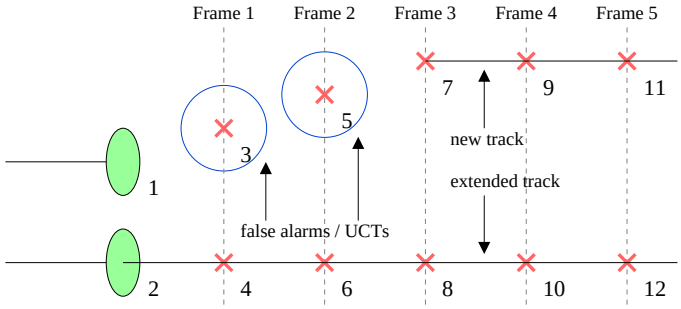

Figure 2. Tracks, UCTs, and false alarms generated by running an MHT without maneuver detection.

STATEMENT OF PROBLEM

We first state the main goals addressed in this paper:

1. Given *point estimates* for an initial and final space object track state, compute the fuel-optimal control cost and control profile, while keeping the framework as general as possible.
2. Given *uncertainties* in said initial and final states, compute the distribution of the fuel-optimal control cost.
3. Formulate a hypothesis test for maneuver feasibility, and a test for scoring UCT associations/correlations based on the distribution of the fuel-optimal control cost.

Further, the key assumptions we make in the paper are the following:

1. We are given full 6-D track states (e.g. as output of an orbit determination process).
2. Any maneuvers conducted by space objects, in the absence of any other knowledge, are conducted in a *fuel-optimal* manner.
3. In the absence of any data other than the track states, candidate UCT associations/correlations are scored based on the "control distance" or the "fuel-cost distance." That is, the association with the lowest possible fuel cost is assumed to be the correct one.

We now briefly formalize the notion of determining if a maneuver is physically realistic in terms of fuel cost. The optimal control computation that will be described shortly connects two point

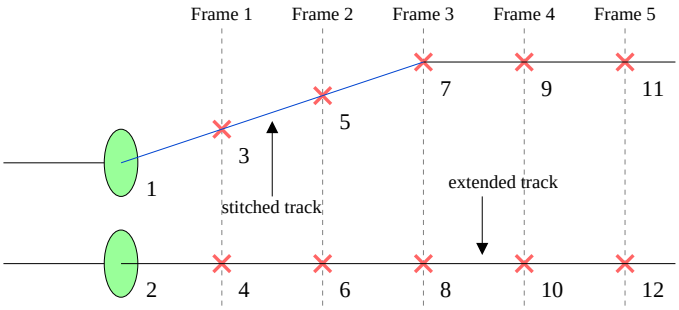

Figure 3. The result of applying a post-processor track stitching algorithm to connect disparate tracks, UCTs, and false alarms by way of an optimal control.

state estimates $\boldsymbol{x}(t_0)$ and $\boldsymbol{x}(t_f)$. In practice, these state estimates would usually be the output of a batch estimation (orbit determination) process, and thus would have some uncertainty associated with them. We assume that the initial state is a Gaussian random variable $\boldsymbol{X}_0 \sim \mathcal{N}(\boldsymbol{x}_0, \mathbf{P}_0)$, the final state is $\boldsymbol{X}_f \sim \mathcal{N}(\boldsymbol{x}_f, \mathbf{P}_f)$, and the joint distribution of $\boldsymbol{X}_0$ and $\boldsymbol{X}_f$ or, equivalently, of $\boldsymbol{X} \equiv (\boldsymbol{X}_0, \boldsymbol{X}_f)$, is $\boldsymbol{X} \sim \mathcal{N}(\boldsymbol{\mu}, \mathbf{P})$, where $\boldsymbol{\mu} = (\boldsymbol{x}_0, \boldsymbol{x}_f)$, $\mathbf{P} = \mathrm{diag}(\mathbf{P}_0, \mathbf{P}_f)$. Our goal in this paper is to compute the distribution of $\Delta V \equiv \Delta V(\boldsymbol{X})$, which is a complicated transformation since the mapping involves solving an optimal control problem. Once a CDF for the ΔV random variable is obtained, we calculate $P(\Delta V \leqslant \Delta V^{\mathrm{th}})$ for some ΔV^{th} determined by the user. The larger this probability, the more feasible the maneuver is understood to be. In addition, this probability is understood to be a crude estimate of the "probability of a maneuver."

The end goal is to incorporate this framework for dealing with maneuvering spacecraft practically within a multiple hypothesis tracking (MHT) framework.[2] A full discussion of MHT is outside the scope of this paper, but what follows is a brief discussion of a method for joint association and maneuver detection based on "track stitching" which has the computational advantage that disparate tracks and UCTs can be stitched or pieced together using the optimal control approach as an *offline post-processor* to the MHT. In this approach, we first process the tracks and reports through a standard MHT ignoring the possibility of any maneuvers. If tracking actual maneuvering targets, this first pass will inevitably generate broken tracks and UCTs. For example, if the reports in the scenario of Figure 1 are processed through an MHT in this manner (note that the quiescent model in this example is motion along a horizontal line), then track '1' would not receive any updates over the five frames of data, a new track would be initiated in Frame 3 beginning with report '7', and reports '3' and '5' would be declared UCTs (if they are full rank states) or false alarms (if they are lower-dimensional observations). These results are depicted in Figure 2. Next, as a post-processor, all of the broken tracks and false alarms (reports '1', '3', and '5' in this example) are gathered and we then determine if they could be stitched together or linked amongst themselves or to any initiated tracks (track $7 \rightarrow 9 \rightarrow 11$ in this example) by way of an optimal control. Before even attempting to solve such a nonlinear control problem, we would use a cheaper maneuver detection algorithm, such as an impulsive maneuver filter model with process noise, to rule out any unlikely maneuver hypotheses. For those hypotheses that remain, the optimal control cost distribution would then be computed to assess if a maneuver is physically realistic. For example, referring once again to Figure 2, a feasible optimal control might exist between reports '1' and '3'; the two reports would then be stitched or fused together using a standard filter propagation algorithm (e.g., the UKF) in conjunction with the nominal dynamical model and the computed optimal control. This process would be repeated on the stitched track $1 \rightarrow 3$ and report '5'. What could result by applying the

track stitching methodology to this simple example is depicted in Figure 3. Two tracks (without breaks) are obtained and reports '3' and '5', originally declared to be UCTs, are resolved. We next dicuss the dynamical model and cost functions used in our optimal control framework.

DYNAMICS AND CONTROL COST FUNCTIONS

In our framework, we use a general Newtonian dynamical model with respect to Cartesian Earth-Centered Inertial (ECI) position-velocity coordinates, with propulsive thrust arising linearly in the equations. The general form is given by the ordinary differential equation

$$\boldsymbol{x}'(t) = \boldsymbol{f}(\boldsymbol{x}(t), \boldsymbol{u}(t), t) \equiv \boldsymbol{f}_d(\boldsymbol{x}(t), t) + \mathbf{B}(\boldsymbol{x}(t), t)\, \boldsymbol{u}(t),$$

where $\boldsymbol{u} \in \mathbb{R}^3$ is the thrust control input, $\mathbf{B} \in \mathbb{R}^6 \times \mathbb{R}^3$, and $\boldsymbol{f}_d : \mathbb{R}^6 \times \mathbb{R} \to \mathbb{R}^6$ are the (ballistic) equations of motion of the system*. In principle, we could use an object-specific thrust model if the object type was known.

As mentioned above, a common control effort metric used in spacecraft maneuver applications to assess fuel cost is the total velocity increment ΔV. Assuming that $\boldsymbol{u}$ is in units of acceleration (which should be the case if it is modeled as a thrust input as described above), the total ΔV effort over a time interval is simply the integrated thrust magnitude over the interval:

$$\Delta V = \|\boldsymbol{u}(t)\|_{L_1} = \int_{t_0}^{t_f} \|\boldsymbol{u}(t)\|_2 \, \mathrm{d}t = \int_{t_0}^{t_f} \sqrt{\boldsymbol{u}(t)^T \boldsymbol{u}(t)} \, \mathrm{d}t. \tag{1}$$

While minimum ΔV problems have been studied in the literature for special cases of maneuvers, they have been avoided in general settings, partly because the integrand in the ΔV definition above is non-differentiable near the zero-thrust case (which leads to numerical difficulties in optimization problems when transitioning from zero-thrust to low-thrust solutions). For example, a more mathematically tractable alternative often used is the quadratic cost,

$$P = \frac{1}{2}\|\boldsymbol{u}(t)\|_{L_2}^2 = \frac{1}{2}\int_{t_0}^{t_f} \boldsymbol{u}(t)^T \boldsymbol{u}(t) \, \mathrm{d}t, \tag{2}$$

which is often interpreted as a total energy.[3] Throughout the paper, the term "L_1-cost" is used interchangeably with "ΔV cost", and "L_2-cost" is used interchangeably with "energy cost" or "quadratic cost." The reader is also referred to Ref. [6] for an overview of the relation between the L_1 and L_2 optimal control problem. We note that P can be used to construct an upper bound on the ΔV cost via the Cauchy-Schwartz inequality: $\Delta V \leqslant \sqrt{2P(t_f - t_0)}$. This bound, however, is often quite loose (e.g., in case of long time intervals). Also, more crucially for the purpose of ranking control costs for different scenarios, an L_1-optimal cost ranking may not be preserved under the L_2 cost. That is, consider two scenarios A and B, and let $\Delta V^{\mathrm{opt}}_{L_1,A}$ and $\Delta V^{\mathrm{opt}}_{L_1,B}$ denote their L_1-optimal ΔV costs. Similarly, let the optimal quadratic costs be denoted as $\Delta V^{\mathrm{opt}}_{L_2,A}$ and $\Delta V^{\mathrm{opt}}_{L_2,B}$. Then, an ordering $\Delta V^{\mathrm{opt}}_{L_1,A} \leqslant \Delta V^{\mathrm{opt}}_{L_1,B}$ does not necessarily imply that $\Delta V^{\mathrm{opt}}_{L_2,A} \leqslant \Delta V^{\mathrm{opt}}_{L_2,B}$! A counterexample illustrating this effect is presented later in the results section.

Computing the optimal control law for connecting two state estimates is in general a nonlinear continuous-time optimization problem. In the next section, we discuss our formulation and one specific method of solving the resulting problem.

*If $\boldsymbol{x} = (x, y, z, \dot{x}, \dot{y}, \dot{z})$ denotes ECI coordinates, then $\mathbf{B} = [\mathbf{0}_{3\times3}, \mathbf{I}_{3\times3}]^T$.

CONTINUOUS-TIME OPTIMAL CONTROL

We begin by specifying the form of our optimal control problem. Let $\boldsymbol{x}(t)$ and $\boldsymbol{u}(t)$ denote the state and control, respectively, at time t. For notational convenience, we will suppress the time dependence when it is clear from context. The optimization problem is

$$\begin{aligned} \underset{\boldsymbol{x},\boldsymbol{u}}{\text{Minimize}} \quad & \Delta V = \int_{t_0}^{t_f} \sqrt{\boldsymbol{u}(t)^T \boldsymbol{u}(t)}\, \mathrm{d}t \\ \text{Subject To} \quad & \boldsymbol{x}'(t) = \boldsymbol{f}(\boldsymbol{x}(t), \boldsymbol{u}(t), t), \\ & \boldsymbol{g}(\boldsymbol{x}(t_0), \boldsymbol{x}(t_f)) = \boldsymbol{0}. \end{aligned} \tag{3}$$

In a more general setting, we can also have path constraints on the state and control. We will not consider path constraints for our present application (the methods, however, easily carry over if we do). We consider fully specified initial and final states ($\boldsymbol{x}_0$ and $\boldsymbol{x}_f$, respectively) at fixed initial and final times as our boundary conditions. Thus, the function $\boldsymbol{g}$ is the following:

$$\boldsymbol{g}(\boldsymbol{x}(t_0), \boldsymbol{x}(t_f)) = \begin{bmatrix} \boldsymbol{x}(t_0) - \boldsymbol{x}_0 \\ \boldsymbol{x}(t_f) - \boldsymbol{x}_f \end{bmatrix}.$$

In general, instead of a final state, we may have a final measurement boundary condition $\boldsymbol{z}(t_f) = \boldsymbol{h}(\boldsymbol{x}(t_f))$, where $\boldsymbol{h}$ is the measurement function. The problem in (3) is a very general nonlinear optimal control problem and, as such, has been studied extensively in the control theory literature. The traditional approach from calculus of variations[10] is to apply the Pontryagin minimum principle, where the continuous necessary conditions for optimality are first derived and a resulting two-point boundary value problem is solved. The approach we take here belongs to a more recent and increasingly popular class of methods that have come to be known as "direct" methods. The general idea in direct methods for optimal control involves a discretization of the original continuous-time problem that results in a nonlinear programming (NLP) problem,[11] which is then solved via known NLP solution techniques such as sequential quadratic programming (SQP) or interior point methods. In what follows, we briefly discuss the discretization method and the resulting NLP formation for our control problem. We acknowledge that the treatment here has been adapted from Refs. [12,13] to our specific problem. Finally, we also acknowledge the work done by Holzinger and Scheeres,[3] where they use an indirect approach to compute energy-optimal trajectories (as opposed to fuel-optimal trajectories).

Huber Approximation to the ΔV Objective

As noted above, the ΔV objective function is non-differentiable at $\boldsymbol{u} = \boldsymbol{0}$ and, as a result, traditional "indirect" methods are difficult to apply. In our "direct" transcription approach, however, we can directly use a smooth approximation to the true objective function. Specifically, we propose to apply the Huber approximation:[7]

$$L(\boldsymbol{u}; \epsilon) = \begin{cases} \|\boldsymbol{u}\|_2, & \text{if} \quad \|\boldsymbol{u}\|_2 > \epsilon, \\ \alpha \|\boldsymbol{u}\|_2^2 + \beta, & \text{if} \quad \|\boldsymbol{u}\|_2 \leqslant \epsilon. \end{cases}$$

For smoothness, we choose $\alpha = \frac{1}{2\epsilon}$ and $\beta = \frac{\epsilon}{2}$. A choice of $\epsilon = 10^{-8}$ was found to be appropriate for our purpose here and it is assumed henceforth. Our results show that the resulting approximation provides a control solution that is very close to optimal in terms of ΔV. As a result, we obtain more accurate estimates of the ΔV effort required to connect two given states. In addition,

for well-studied simple maneuvers, the control profiles obtained via our approximation are very similar to known analytical solutions. Due to the piecewise definition of the Huber approximation, for notational convenience we will refer to the integrand in the ΔV cost functional (1) as simply $L(\boldsymbol{u}; \epsilon)$.

Gauss Pseudospectral Discretization and NLP Formulation

As mentioned above, the first step in a "direct" solution method is to discretize the original continuous-time problem into a NLP. Choice of an appropriate discretization scheme for forming a NLP is critical and several schemes have been studied in the control theory literature. For our results here, we use the Gauss pseudospectral (GS) discretization framework,[14] one of several orthogonal collocation methods used in direct methods for optimal control. The overall scheme has three key advantages: (i) it leads to efficient approximations to the integral defining the cost, the differential equation constraint, and the path constraints; (ii) it provides an accurate estimate of the costate which provides an equivalence with traditional indirect methods[10] and facilitates a sensitivity analysis of the extremal trajectory; and (iii) it provides a convenient way to address the non-smoothness of the ΔV objective function. This framework is robust and sufficiently general to accommodate the use of higher-order gravity models, non-conservative forces, general boundary conditions and path constraints, spacecraft specific thrust models and parameters (as determined possibly by feature extraction from the observations), and allows use of powerful techniques from nonlinear programming. We now describe the method for discretizing the problem in (3). In what follows, the discretization points t_i, $i = 1, \ldots, N$, are the Legendre-Gauss (LG) points* on the time interval (t_0, t_f); t_0 denotes the endpoint t_0 and t_{N+1} denotes the endpoint t_f. The state $\boldsymbol{x}(t)$ is approximated as

$$\boldsymbol{x}(t) \approx \hat{\boldsymbol{x}}(t) = \sum_{i=0}^{N} \hat{\boldsymbol{x}}(t_i)\ell_i(t), \tag{4}$$

where $\ell_i(t)$, $i = 0, \ldots, N$, are the Lagrange interpolating polynomials defined as

$$\ell_i(t) = \prod_{j=0, j\neq i}^{N} \frac{t - t_j}{t_i - t_j}. \tag{5}$$

The control $\boldsymbol{u}(t)$ is discretized in a similar fashion, with one key difference being that it is not approximated directly at the endpoint t_0:

$$\boldsymbol{u}(t) \approx \hat{\boldsymbol{u}}(t) = \sum_{i=1}^{N} \hat{\boldsymbol{u}}(t_i)\ell_i^*(t), \tag{6}$$

where again

$$\ell_i^*(t) = \prod_{j=1, j\neq i}^{N} \frac{t - t_j}{t_i - t_j} \tag{7}$$

are the Lagrange interpolation polynomials (note that the $\ell_i^*(t)$ in (7) are different from the $\ell_i(t)$ in (5) due to the inclusion of the endpoint t_0 in (5)).

*The Legendre-Gauss points are usually provided for the interval $[-1, 1]$ and are precisely the roots of the N^{th}-degree Legendre polynomial. The corresponding LG points on an arbitrary interval can be obtained from those on $[-1, 1]$ through an affine transformation.

Differentiating (4), we obtain the discretization of the state derivative:

$$\boldsymbol{x}'(t) \approx \hat{\boldsymbol{x}}'(t) = \sum_{i=0}^{N} \boldsymbol{x}(t_i) \frac{\mathrm{d}\ell_i(t)}{\mathrm{d}t}.$$

For notational convenience, we denote the derivative of the Lagrange polynomials at the LG points as a differentiation matrix $\mathbf{D} \in \mathbb{R}^{N \times N+1}$, with elements

$$D_{ki} = \ell_i'(t_k), \quad k = 1, \ldots, N, \quad i = 0, \ldots, N. \tag{8}$$

These elements can be determined offline. The continuous-time cost and dynamics can now be approximated using classical Gaussian quadrature methods using the LG points. Putting everything together, we obtain the following finite-dimensional NLP:

$$\begin{aligned} \underset{\hat{\boldsymbol{x}}, \hat{\boldsymbol{u}}, \hat{\boldsymbol{x}}_0, \hat{\boldsymbol{x}}_f}{\text{Minimize}} \quad & \Delta\hat{V} = \sum_{k=1}^{N} w_k \, L(\hat{\boldsymbol{u}}_k; \epsilon) \\ \text{Subject To} \quad & \hat{\mathbf{X}} \boldsymbol{d}_k - \boldsymbol{f}(\hat{\boldsymbol{x}}_k, \hat{\boldsymbol{u}}_k, t_k) = \mathbf{0}, \quad k = 1, \ldots, N, \\ & \hat{\boldsymbol{x}}_f = \hat{\boldsymbol{x}}_0 + \sum_{k=1}^{N} w_k \boldsymbol{f}(\hat{\boldsymbol{x}}_k, \hat{\boldsymbol{u}}_k, t_k), \\ & \boldsymbol{g}(\hat{\boldsymbol{x}}_0, \hat{\boldsymbol{x}}_f) = \mathbf{0}. \end{aligned} \tag{9}$$

Here, w_k are the LG quadrature weights, t_k are the LG points, $\hat{\mathbf{X}}$ is the matrix with $\hat{\boldsymbol{x}}_1, \ldots, \hat{\boldsymbol{x}}_N$, as its columns, $\boldsymbol{d}_k^T$ denotes the k^{th} row of the differentiation matrix $\mathbf{D}$, $\hat{\boldsymbol{x}}_k \equiv \hat{\boldsymbol{x}}(t_k) \in \mathbb{R}^6$, and $\hat{\boldsymbol{u}}_k \equiv \hat{\boldsymbol{u}}(t_k) \in \mathbb{R}^3$. Further, $\hat{\boldsymbol{x}}_0 \equiv \hat{\boldsymbol{x}}(t_0)$ and $\hat{\boldsymbol{x}}_f = \hat{\boldsymbol{x}}(t_f) = \hat{\boldsymbol{x}}(t_{N+1})$. Note that $\hat{\boldsymbol{x}}_f$ is not a collocated point and is instead defined in terms of $\hat{\boldsymbol{x}}_0$ via the discretized dynamics; this results in the second constraint in (9). The end goal for this NLP formulation is to be able to use powerful techniques from nonlinear programming to get accurate approximations to a solution to the original continuous-time problem. An advantage of the particular discretization procedure described here is that accurate costate estimates can be obtained from the Lagrange multipliers arising in the Karush-Kuhn-Tucker (KKT)[11] conditions of the NLP. A costate mapping theorem that formalizes this is provided in Ref. [12].

TREATMENT OF UNCERTAINTY IN THE BOUNDARY CONDITIONS

The optimal control computation described in the previous sections connects two point state estimates $\boldsymbol{x}(t_0)$ and $\boldsymbol{x}(t_f)$. In practice, these state estimates would usually be the output of a batch estimation (orbit determination) process, and thus would have some uncertainty associated with them. As already discussed in the problem statement section, we wish to compute the distribution of $\Delta V \equiv \Delta V(\boldsymbol{X})$, which is a complicated transformation since the mapping involves solving an optimal control problem. We note again here that $\boldsymbol{X} \sim \mathcal{N}(\boldsymbol{\mu}, \mathbf{P})$, where $\boldsymbol{X} \equiv (\boldsymbol{X}_0, \boldsymbol{X}_f)$. Further, $\boldsymbol{X}_0 \sim \mathcal{N}(\boldsymbol{x}_0, \mathbf{P}_0)$ is the initial state distribution, $\boldsymbol{X}_f \sim \mathcal{N}(\boldsymbol{x}_f, \mathbf{P}_f)$ is the final state distribution, and $\boldsymbol{\mu} = (\boldsymbol{x}_0, \boldsymbol{x}_f)$ and $\mathbf{P} = \mathrm{diag}(\mathbf{P}_0, \mathbf{P}_f)$.

Computing a Representation for the Control Cost Distribution

The Unscented Transform and Gauss-Hermite Quadrature The overview here is taken from the more detailed treatment provided in Ref. [15]. The unscented transform[9,16] and Gauss-Hermite

(GH) quadature rules are intimitely related. Starting with the n-variate Gaussian $\boldsymbol{X} \sim \mathcal{N}(\boldsymbol{\mu}, \mathbf{P})$ ($n = 12$ in our case) and a nonlinear transformation $\boldsymbol{f} : \mathbb{R}^n \to \mathbb{R}^n$, the unscented transform approximates the mean and covariance of the transformed variable $\boldsymbol{f}(\boldsymbol{X})$ correct to third-order. In other words, the unscented transform provides a means of integrating the function $\boldsymbol{f}$ multiplied by a Gaussian weight function. Gauss-Hermite quadrature effectively approximates the integral by evaluating the function $\boldsymbol{f}$ at strategically chosen sigma points (or nodes) and then taking a weighted average.

Families of GH quadrature rules for integration over $\mathbb{R}$ can be readily derived using the Golub-Welsch algorithm[17] as follows. Let $\mathbf{J} \in \mathbb{R}^{m \times m}$ be the tridiagonal symmetric matrix with $J_{\alpha,\alpha+1} = J_{\alpha+1,\alpha} = \sqrt{\alpha}$, $\alpha = 1, \ldots, m-1$, and $J_{\alpha,\alpha} = 0$, $\alpha = 1, \ldots, m$. Then,

$$\frac{1}{\sqrt{2\pi}} \int_{-\infty}^{\infty} \mathrm{e}^{-\frac{1}{2}x^2} f(x)\, \mathrm{d}x \approx \sum_{\alpha=1}^{m} w_\alpha f(x_\alpha), \tag{10}$$

is a $(2m-1)$-th order accurate quadrature rule (i.e., it is exact if $f(x)$ is any polynomial up to and including degree $2m-1$). Here, the nodes x_α are the eigenvalues of $\mathbf{J}$ while the weights w_α are given by $[(\boldsymbol{v}_\alpha)_1]^2$, where $(\boldsymbol{v}_\alpha)_1$ is the first component of the α-th normalized eigenvector of $\mathbf{J}$. A quadrature rule in n dimensions can be formed by taking the n-fold Cartesian product of the one-dimensional GH rule so that

$$\frac{1}{(2\pi)^{n/2}} \int_{\mathbb{R}^n} \mathrm{e}^{-\frac{1}{2}\boldsymbol{x}^T\boldsymbol{x}} \boldsymbol{f}(\boldsymbol{x})\, \mathrm{d}^n\boldsymbol{x} \approx \sum_{\alpha_1=1}^{m} \cdots \sum_{\alpha_n=1}^{m} w_{\alpha_1} \cdots w_{\alpha_n}\, \boldsymbol{f}(x_{\alpha_1}, \ldots, x_{\alpha_n}). \tag{11}$$

By an affine change of variable, functions multiplied by an arbitrary Gaussian weight function can also be integrated:

$$\mathrm{E}[\boldsymbol{f}(\boldsymbol{X})] = \int_{\mathbb{R}^n} \mathcal{N}(\boldsymbol{x}; \boldsymbol{\mu}, \mathbf{P})\, \boldsymbol{f}(\boldsymbol{x})\, \mathrm{d}^n\boldsymbol{x} \approx \sum_{\boldsymbol{x}_\alpha \in \Omega} w_\alpha \boldsymbol{f}(\boldsymbol{\mu} + \mathbf{A}\boldsymbol{x}_\alpha). \tag{12}$$

In (12), $\Omega \subset \mathbb{R}^n$ denotes the set of GH nodes, w_α is the weight associated to the α-th node in Ω, and $\mathbf{P} = \mathbf{A}\mathbf{A}^T$. The set $\{\boldsymbol{\mu} + \mathbf{A}\boldsymbol{x}_\alpha\}_{\boldsymbol{x}_\alpha \in \Omega}$ is precisely the set of sigma points for a Gaussian with mean $\boldsymbol{\mu}$ and covariance $\mathbf{P}$. This connection between GH quadrature rules and the unscented sigma points was also observed by Ito and Xiong.[18]

The quadrature schemes (11) and (12) are order $2m-1$ accurate but require m^n function evaluations when the Cartesian product node set Ω is used. This establishes the curse of dimensionality; for fixed order, the number of nodes grows *exponentially* with dimension. The choice of more efficient node sets Ω, in particular, ones in which the cardinality grows *polynomially* with dimension, is thus of primary importance in quadrature theory and ultimately in the implementation of an efficient GH (i.e., higher-order unscented) filter.

Multidimensional Gauss-Hermite quadrature schemes which have a minimal number of nodes required to achieve a given accuracy are developed by Genz and Keister[19] (GK). The resulting quadrature rules* enjoy the property that the number of nodes grows only polynomially with dimension when the order is fixed. For example, the number of nodes (sigma points) for third- and fifth-order GH-GK quadrature methods is $2n+1$ and $2n^2+1$, respectively. In contrast, these numbers become 2^n and 3^n, respectively, when the naive Cartesian product node set is assumed.

*The Genz-Keister nodes and weights can be downloaded at http://sparse-grids.de.

In our approach here, we first estimate the mean and variance of the transformation $\Delta V(\boldsymbol{X}_0, \boldsymbol{X}_f)$, and then fit a shifted Gamma distribution via moment matching. The first and second moments of the ΔV random variable are estimated as

$$\hat{\mu}_{\Delta V} = \sum_{\boldsymbol{x}_i \in \Omega} w_i \Delta V(\boldsymbol{x}_i), \tag{13}$$

and

$$\hat{\sigma}^2_{\Delta V} = \sum_{\boldsymbol{x}_i \in \Omega} w_i (\Delta V(\boldsymbol{x}_i) - \hat{\mu}_{\Delta V})^2, \tag{14}$$

In the results section, we show several examples using fifth-order (289 σ-points) and seventh-order (2097 σ-points) Gauss-Hermite quadrature. For comparison, we also show the histogram of the ΔV-optimal cost computed from 10,000 independent Monte Carlo (MC) runs. Note, however, that the MC runs are only computed to more accurately approximate "truth." We would never try to estimate the Gamma distribution parameters using such a large MC sample as it would be computationally infeasible in an online setting. The unscented transform, on the other hand, is computationally feasible, since not only do we have a reduced set of sample points, we also have a good estimate of the optimal control and ΔV cost for each σ-point based on the nominal trajectory. Warm starting the NLP with this solution makes the solution much easier to obtain as the number of iterations is significantly reduced.

Fitting a Parametric Distribution

For the results presented in this paper, we fit a shifted Gamma distribution to the computed first two moments of the ΔV random variable via Gauss-Hermite quadrature as defined in (13) and (14). Specifically, we use simple moment matching to fit the shape and scale parameters of a Gamma distribution (the choice of fitting a Gamma distribution was made after qualitative goodness-of-fit experiments with several popular parametric distributions). That is, we approximate the distribution of the ΔV random variable as $\Delta V \sim \Gamma(k, \theta, \delta)$, where $k > 0$ is the shape parameter, $\theta > 0$ is the scale parameter, $\delta > 0$ is the shift parameter, and

$$\Gamma(x; k, \theta, \delta) = \begin{cases} (x-\delta)^{k-1} \frac{e^{-(x-\delta)/\theta}}{\Gamma(k)\theta^k}, & x > \delta \\ 0, & x < \delta \end{cases} \tag{15}$$

The shift parameter δ is taken to be the nominal control cost (the cost connecting the mean initial and final states). By moment matching, the parameters k and θ satisfy $k\theta + \delta = \hat{\mu}_{\Delta V}$ and $k\theta^2 = \hat{\sigma}^2_{\Delta V}$.

Testing for Maneuver Feasibility and Comparing Candidate UCT Associations

The proposed hypothesis test for determining feasibility of a maneuver is a test between the null hypothesis $\mathcal{H}_0$ that the maneuver is feasible and the alternate hypothesis $\mathcal{H}_a$ that the maneuver is infeasible. Further, we decide that

- $\mathcal{H}_0$ is accepted if $P(\Delta V \leqslant \Delta V^{\text{th}}) \geqslant 1 - \alpha$, (otherwise $\mathcal{H}_0$ is rejected),

where α is a significance level (e.g., 0.05), and ΔV^{th} is a threshold chosen by the operator.

For scoring (and hence, ranking) UCT associations based on maneuver feasibility, the ideal method is to incorporate the measure of maneuver feasibility into the likelihood scores that are

an integral component of a MHT. A rigorous derivation of the likelihood ratios for scoring is given in Poore[2] and will be not be repeated here. We note in particular that $P_A(\Delta V \leqslant \Delta V^{\text{th}})$ is to be viewed as the "probability of a maneuver" (in the absence of any other predictors/variables that may indicate information about possible maneuvers), and this term would arise as part of the likelihood ratios in a MHT track stitching stage (in addition to the prediction error term). For a simplistic comparison that we use here, the following is used to compare a candidate UCT pairing A with a candidate pairing B, in the absence of any other data and all aspects (except for the optimal control profile and cost behavior) being equal for the candidate pairings:

- UCT pair A wins over pair B if $P_A(\Delta V \leqslant \Delta V^{\text{th}}) > P_B(\Delta V \leqslant \Delta V^{\text{th}})$.

Equivalently, we use the CDF of the fitted Gamma distribution to compute UCT pairing scores. Note that the above comparison assumes a fixed ΔV^{th}. The inequality may not hold for all possible values of ΔV^{th}. At the end of the results section, it will be shown that accurate estimates of the control cost distribution are critical in this framework for making the right correlation decision. In particular, using different cost functionals (e.g., using quadratic cost instead of the ΔV cost) could result in different associations.

RESULTS

We now present results on several simulated scenarios to validate the above outlined methodology for the nominal control computations and treatment of uncertainties via the unscented transform. We also show a simple UCT association scenario, in which using the computational easier L_2 optimal control framework instead of the more physically realistic L_1 cost can lead to a wrong association.

In all scenarios, we simulate a set of "truth" trajectories consisting of an initial and final state, and attempt to recover the ΔV-optimal controls (and their distributions) that connects the two states. The mean initial state $\boldsymbol{x}_0$ is a *circular, non-inclined orbit in GEO*, with instantaneous orbital period of 24 hours. The mean final state $\boldsymbol{x}_f$ is generated by propagating $\boldsymbol{x}_0$ for 24 hours, with a maneuver occurring during part of the propagation interval. We use a degree and order 70 gravity model to simulate the initial and final conditions in all scenarios. Unless indicated otherwise, the states are represented in ECI coordinates with length in units of Earth radii (ER) and time in units of hours.

Nominal ΔV-Optimal Control Computation

To test and validate the Gauss pseudospectral approach combined with the Huber approximation to the L_1 cost, we consider the following scenarios:

- *Nominal control computation scenarios.* In Scenarios 1_{imp}, 2_{imp}, and 3_{imp}, an impulsive maneuver of magnitude $\Delta V_{true} = 2\,\text{m/s}$ is conducted along the z-direction at $t = 0, 24$, and $12\,\text{hr}$, respectively. Scenario 4_{imp} is defined analogously with an impulse time at $t = 15\,\text{hr}$ and $\Delta V_{true} = 5\,\text{m/s}$. In Scenarios 1_{sb}, 2_{sb}, and 3_{sb}, a constant thrust slow-burn maneuver of magnitude $10^{-7}\,\text{km/s}^2$ is conducted along the radial direction over the intervals $[0, 24\,\text{hr}]$, $[0, 12\,\text{hr}]$, and $[12\,\text{hr}, 24\,\text{hr}]$, respectively. Scenario 4_{sb} is identical to Scenario 1_{sb} but uses a larger thrust of $10^{-6}\,\text{km/s}^2$.

We use the open-source General Pseudospectral Optimal Control Software (GPOPS)[20] to transcribe our control problem (using $N = 30$ LG points) into an NLP as described in the previous

Table 1. Computed values of ΔV using the $J = P$ (energy) and $J = \Delta V$ (total velocity increment) cost functions.

Scenario	ΔV_{true} (m/s)	$\Delta V_{est,J=P}$ (m/s) 31 LG pts	$\Delta V_{est,J=P}$ (m/s) 61 LG pts	$\Delta V_{est,J=\Delta V}$ (m/s) 31 LG pts	$\Delta V_{est,J=\Delta V}$ (m/s) 61 LG pts
1_{imp}	2	2.6112	2.6044	2.0460	2.0465
2_{imp}	2	2.6115	2.6046	2.0462	2.0467
3_{imp}	2	2.4993	2.5031	1.9702	1.9666
4_{imp}	5	6.1965	6.1957	4.8743	4.8686
1_{sb}	8.64	8.6311	8.6311	8.6296	8.6299
2_{sb}	4.32	4.7426	4.7426	4.3113	4.3117
3_{sb}	4.32	4.6662	4.6661	4.3129	4.3129
4_{sb}	86.4	86.3756	86.3756	86.3671	86.3671

section, and use the general purpose solver SNOPT[21] to solve the NLP via sequential quadratic programming. The NLP solved in all simulations uses ECI coordinates and a J_2 gravity model.

For all scenarios here, we compare the optimally estimated ΔV effort with the true ΔV effort. For the impulsive maneuver scenarios, we simply use the impulse magnitude as the ΔV_{true}. For the constant thrust scenarios, we compute the ΔV_{true} by simply integrating the thrust magnitude over the given time interval via $\Delta V_{true} = \int_{t_0}^{t_f} A \, \mathrm{d}t = A(t_f - t_0)$, where A is the constant thrust magnitude. In order to compare to prior work of Holzinger and Scheeres,[3] we also solve the analogous control problem using the energy (2) as the cost function.

Table 1 lists the computed values of ΔV obtained by solving the two different control problems. We denote the ΔV estimate obtained from the ΔV solution as $\Delta V_{est,J=\Delta V}$, and the estimate obtained from the minimum energy solution by $\Delta V_{est,J=P}$. The table also compares results obtained by using 31 and 61 LG points. In summary, the results obtained by using only 31 LG points is comparable to those obtained using 61 LG points, and the *results match the theoretical prediction very well.* Further, although the minimum energy control problem is easier to solve, it tends to overestimate the actual ΔV by as much as 30%, which can be a significant overestimate for space object maneuvers. The consequence of this is shown in the UCT association scenario later, where using the energy cost functional leads to the wrong association while using the ΔV cost functional leads to the right association.

Figure 4 shows the control functions obtained for Scenario 3_{sb}. The qualitative differences in the control function for the minimum energy and ΔV solutions are significant. While the optimal control for the minimum energy solution is smooth, the minimum ΔV solution implies that the optimal (most fuel efficient) control is a *series of impulsive maneuvers*. Therefore, a slow-burn maneuver is not necessarily fuel efficient in terms of ΔV cost! Similar observations are also apparent in Figure 5 showing the control functions obtained for Scenario 4_{imp}. In addition, one of the impulses in the minimum ΔV solution coincides precisely with the actual time of the maneuver. This observation suggests that one can possibly *infer* the type of maneuver from the optimal control and the computed ΔV.

Comparison with Theory: Inclination/Plane Change Maneuvers Finally, we test our method on the well-studied inclination-only change maneuver. We consider a series of scenarios in which

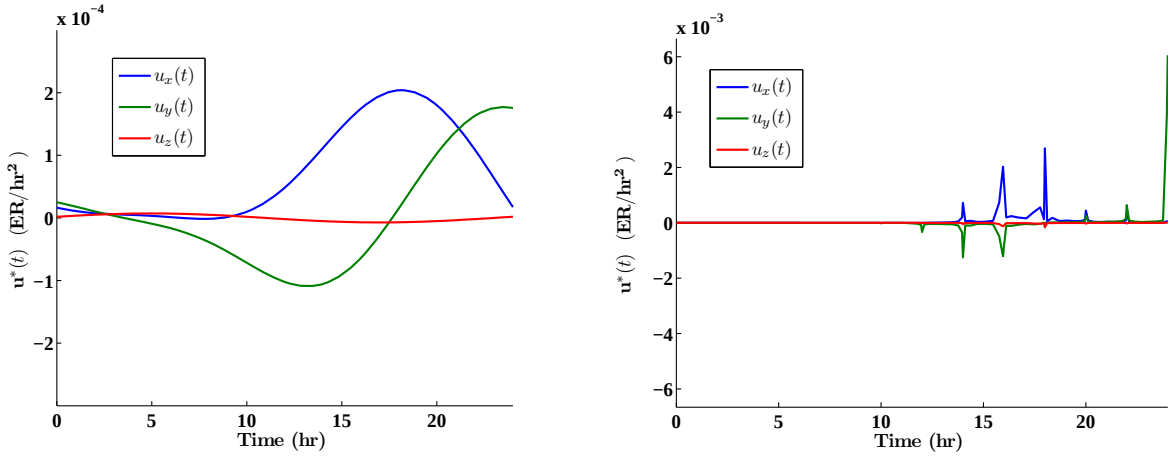

Figure 4. The optimal control profile obtained for Scenario 3_{sb}. Shown are the minimum energy solution (left) and the minimum ΔV solution (right).

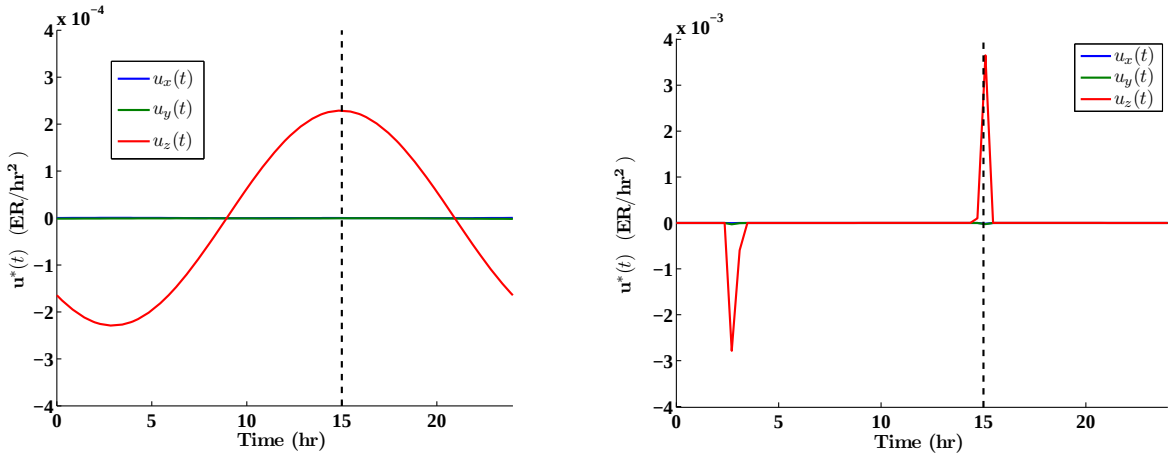

Figure 5. The optimal control profile obtained for Scenario 4_{imp}. Shown are the minimum energy solution (left) and the minimum ΔV solution (right).

the object conducts an impulsive maneuver in the z-direction of magnitude $\Delta V_{true} = 5\,\mathrm{m/s}$ at $t = t_{impulse} \in [0, 24\,\mathrm{hr}]$. With a circular non-inclined orbit as the initial state (as before), and assuming unperturbed Keplerian dynamics, such a maneuver would result in a *change in inclination only*. The optimal ΔV required is given by $\Delta V_{theory} = 2v \sin\left(\frac{\Delta i}{2}\right)$ (see [Ref. 22, §6.4.2]), where Δi is the change in inclination between the initial and final states, and v is the orbital velocity. Figure 6 shows that the theoretically predicted ΔV versus $t_{impulse}$ curve agrees well with estimates obtained from the Huber approximated solution (using as little as 31 LG points), while the estimates obtained from the minimum energy solution are higher by as much as 30%. The sinusoidal shape is due to the fact that the change in inclination Δi itself oscillates as a function of the impulse time $t_{impulse}$ due to the inclusion of higher-order terms in the gravity model. Figure 5 shows an example optimal control profile obtained for such a maneuver.

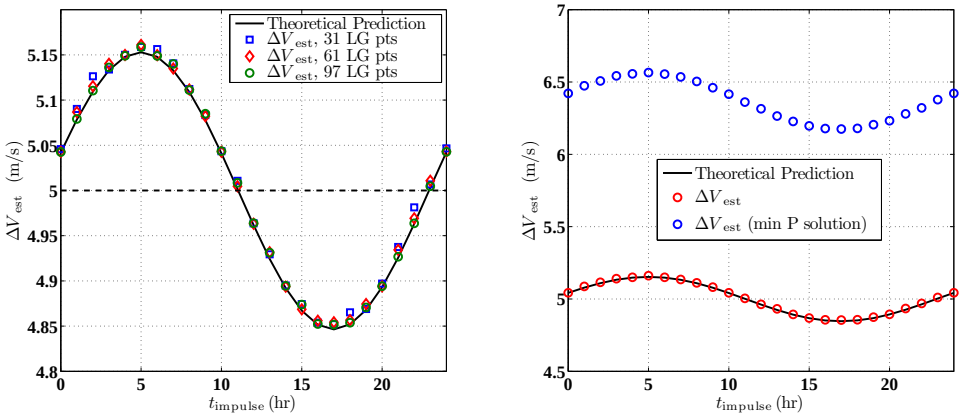

Figure 6. Comparison of ΔV (estimates vs. theoretical prediction) obtained for inclination-only maneuvers (left), and comparison with estimates obtained from minimum "energy" solution (right). The sinusoidal shape is due to the fact that the change in inclination Δi itself oscillates as a function of the impulse time due to the gravity model.

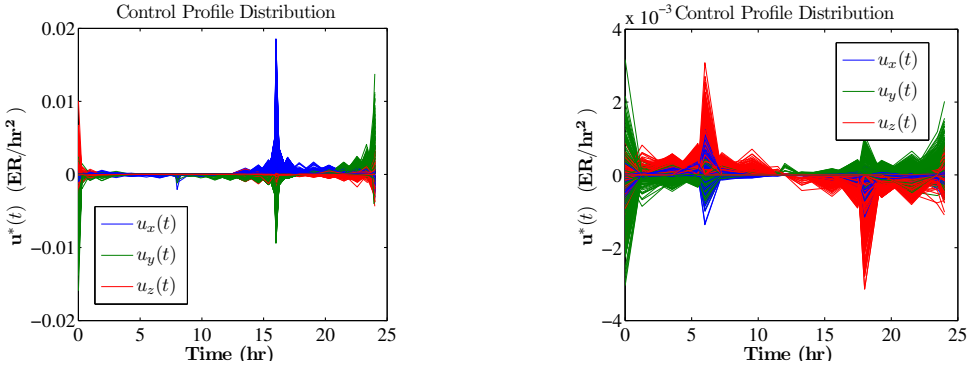

Figure 7. Samples of ΔV-optimal control profiles for Scenarios 3_{sb} and 10.

ΔV Cost Distribution Computation

In the next set of scenarios, we consider uncertainty in the boundary states. Several sizes of uncertainties are considered to test robustness of the proposed approach based on the unscented transform. Following is a brief description of the scenarios:

- *Control cost distribution computation scenarios.* In Scenarios 1 to 8, an impulsive maneuver of magnitude $\Delta V_{true} = 2\,\mathrm{m/s}$ is conducted along the z-direction at $t = 7\,\mathrm{hr}$. These scenarios differ only in terms of their initial and final state uncertainties, which are provided in Tables 2 and 3. In Scenario 9, no maneuver is conducted, and in Scenario 10, an impulsive maneuver of magnitude $\Delta V_{true} = 5\,\mathrm{m/s}$ is conducted along the z-direction at $t = 7\,\mathrm{hr}$.

The goal in these scenarios is to compute the distribution of the ΔV-optimal control cost connecting the initial and final state distributions. For all cases, the covariance $\mathbf{P} = \mathrm{diag}\left(\sigma_x^2, \sigma_y^2, \sigma_z^2, \sigma_{\dot{x}}^2, \sigma_{\dot{y}}^2, \sigma_{\dot{z}}^2\right)$, with the values given in Tables 2 and 3.

Table 2. Initial state uncertainties

Scenario	σ_x (m)	σ_y (m)	σ_z (m)	$\sigma_{\dot{x}}$ (m/s)	$\sigma_{\dot{y}}$ (m/s)	$\sigma_{\dot{z}}$ (m/s)
1	300	250	225	3.0	3.5	3.5
2	60	30	40	0.4	0.8	0.8
3	3,000	3,000	3,000	1.0	1.0	1.0
4	10,000	10,000	10,000	1.0	1.0	1.0
5	2,000	2,000	2,000	5.0	5.0	5.0
6	10,000	10,000	10,000	5.0	5.0	5.0
7	200	150	100	5.0	1.0	1.0
8	200	150	100	1.0	5.0	1.0
9	150	200	100	1.0	2.0	1.0
10	150	200	100	1.0	2.0	1.0

Table 3. Final state uncertainties

Scenario	σ_x (m)	σ_y (m)	σ_z (m)	$\sigma_{\dot{x}}$ (m/s)	$\sigma_{\dot{y}}$ (m/s)	$\sigma_{\dot{z}}$ (m/s)
1	250	300	250	4.5	5.0	4.0
2	80	60	60	0.6	1.0	1.0
3	3,000	3,000	3,000	1.0	1.0	1.0
4	10,000	10,000	10,000	1.0	1.0	1.0
5	2,000	2,000	2,000	5.0	5.0	5.0
6	10,000	10,000	10,000	5.0	5.0	5.0
7	200	150	100	5.0	1.0	1.0
8	200	150	100	1.0	5.0	1.0
9	200	100	150	1.0	1.0	2.0
10	200	100	150	1.0	1.0	2.0

Figures 8-12 show comparisons between a 10,000 sample Monte Carlo histogram (normalized such that the area under the histogram is unity), and a fifth-order and seventh-order Gauss-Hermite quadrature based Gamma distribution fit. The plots show that the fifth-order fits achieve reasonable accuracy while the seventh-order fits match more closely with the histograms. Further, comparing the spread of the computed ΔV distributions with the state uncertainties in Tables 2 and 3, we see that the variances in the velocity coordinates have a larger effect on the ΔV variances (compare, e.g., Scenarios 4 and 6). Finally, Figure 7 shows samples of the actual optimal control profiles for the slow-burn case in Scenario 3_{sb} and the impulsive maneuver case in Scenario 10, with initial and final state uncertainties equal to those of Scenario 2. As can be seen, the approximate nature of the maneuver can still be reconstructed.

UCT Association Cost Comparision (ΔV vs. Quadratic Cost)

We now consider a simple UCT association scenario. Assume that we have an initial $\boldsymbol{X}_0$ (same as the initial state of all previous scenarios), and two given final states $\boldsymbol{X}_f^1$ and $\boldsymbol{X}_f^2$. In the absence

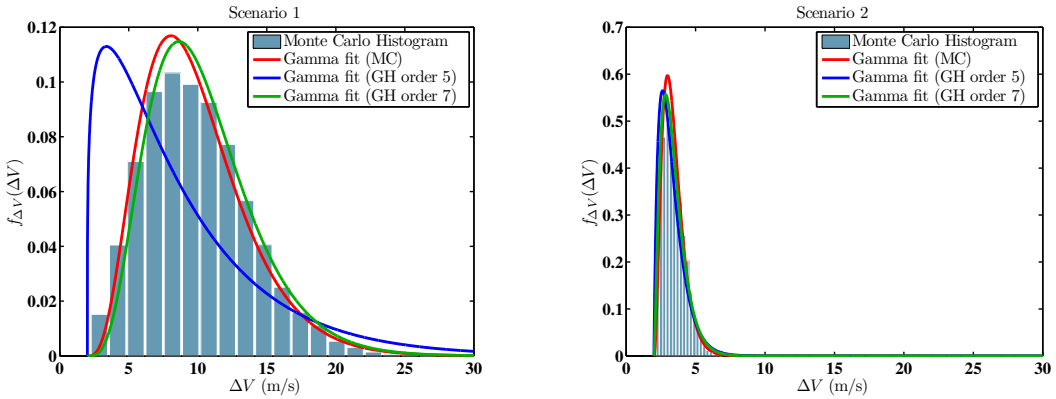

Figure 8. ΔV distributions for Scenarios 1 and 2.

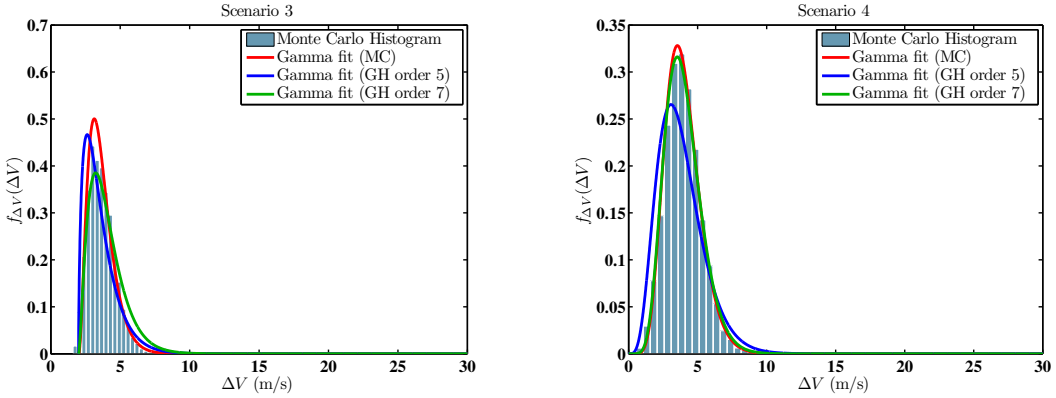

Figure 9. ΔV distributions for Scenarios 3 and 4.

of any other data and all observed and unobserved aspects of the states being equal, we assume that one of $\boldsymbol{X}_f^1$ or $\boldsymbol{X}_f^2$ was generated by the inital state, and apply the UCT association scoring formulation described earlier to determine which association is more feasible in terms of fuel cost (and hence is the correct one by assumption). The results are shown for the case where the mean state $\boldsymbol{x}_f^1$ is identical to the final state of the slow-burn Scenario 3_{sb} described earlier, and the mean $\boldsymbol{x}_f^2$ is the final state obtained by conducting a maneuver of magnitude $\Delta V_{true} = 4\,\mathrm{m/s}$ along the z-direction at $t = 0\,\mathrm{hr}$. The covariances for all states are diagonal. For the initial state $\boldsymbol{X}_0$, we have

$$\sigma_x = 60\ \mathrm{m}, \sigma_y = 30\ \mathrm{m}, \sigma_z = 40\ \mathrm{m}, \sigma_{\dot{x}} = 0.3\ \mathrm{m/s}, \sigma_{\dot{y}} = 0.4\ \mathrm{m/s}, \sigma_{\dot{z}} = 0.4\ \mathrm{m/s},$$

and for both final states $\boldsymbol{X}_f^1$ and $\boldsymbol{X}_f^2$, we have

$$\sigma_x = 80\ \mathrm{m}, \sigma_y = 60\ \mathrm{m}, \sigma_z = 60\ \mathrm{m}, \sigma_{\dot{x}} = 0.6\ \mathrm{m/s}, \sigma_{\dot{y}} = 0.4\ \mathrm{m/s}, \sigma_{\dot{z}} = 0.6\ \mathrm{m/s}.$$

Figures 13 and 14 show the computed PDFs and CDFs for the two possble associations, using the ΔV cost functional and the quadratic cost functional in the optimal control computation (the distribution for the quadratic cost case is still shown in ΔV space however; i.e., the L_1-norm of the L_2-optimal solution is used in computing the distribution). In the figures, the candidate association $\boldsymbol{X}_0 \to \boldsymbol{X}_f^1$ is denoted as $A \to B$, and the candidate association $\boldsymbol{X}_0 \to \boldsymbol{X}_f^2$ is denoted as $A \to C$.

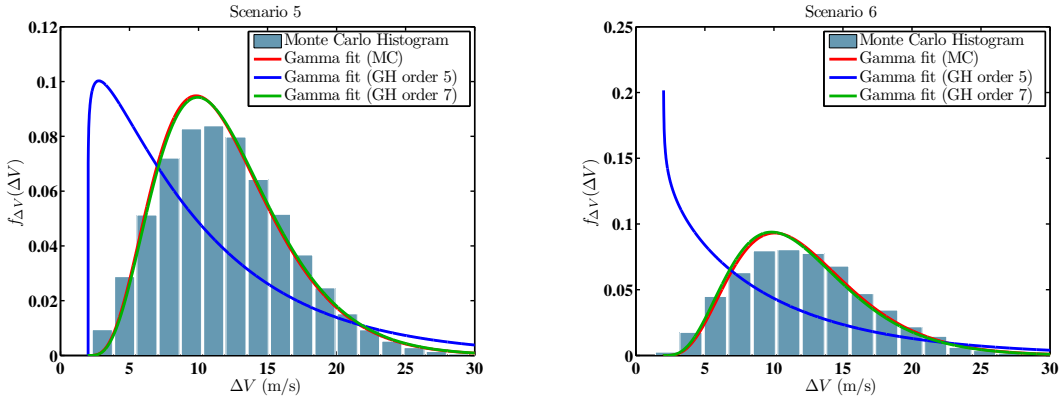

Figure 10. ΔV distributions for Scenarios 5 and 6.

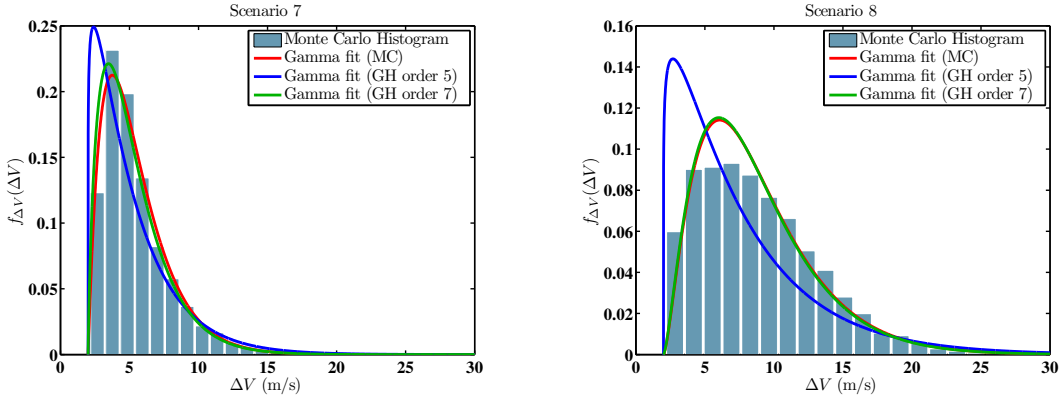

Figure 11. ΔV distributions for Scenarios 7 and 8.

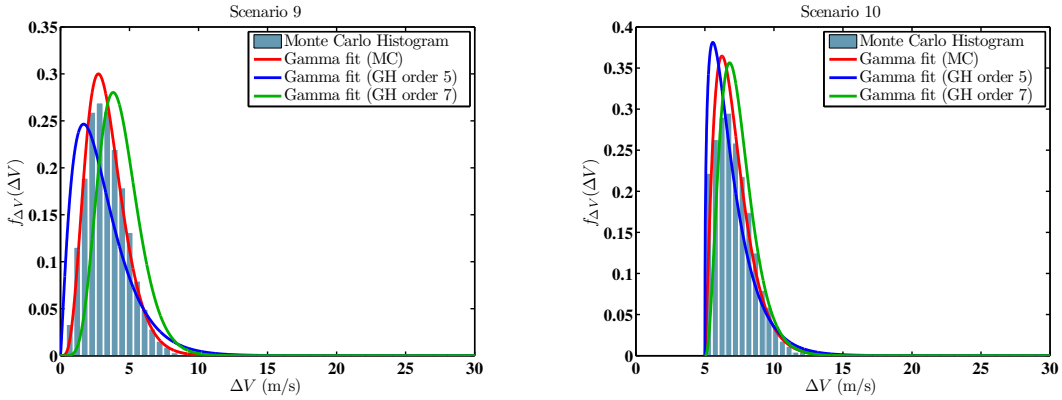

Figure 12. ΔV distributions for Scenarios 9 and 10.

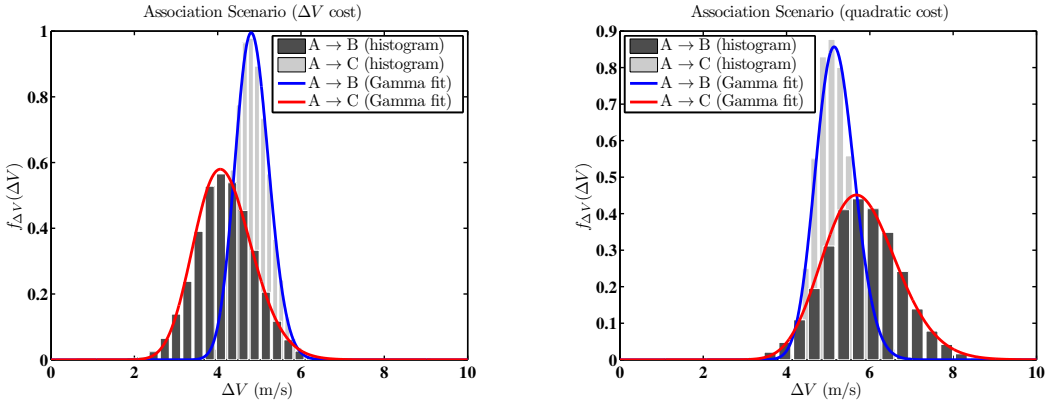

Figure 13. ΔV distributions (PDF) for the UCT association scenarios (Scenarios 11 and 12). The figures show that the order of the distributions for the two candidate pairings switches if quadratic cost is used instead of the ΔV cost.

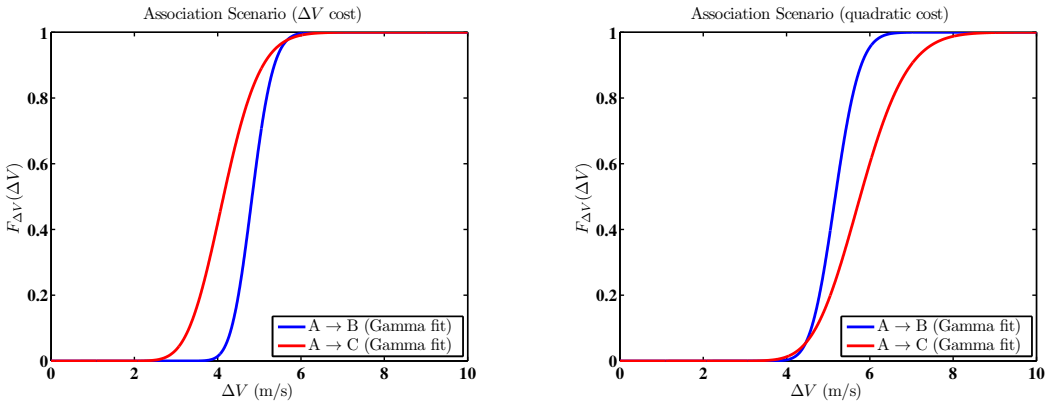

Figure 14. ΔV distributions (CDF) for the UCT association scenarios (Scenarios 11 and 12.

The nominal cost for association $A \to C$ is $4.32\ \mathrm{m/s}$ while the nominal cost for association $A \to B$ is $4\ \mathrm{m/s}$. As can be seen, in this case using the quadratic cost results in switching the order of the two distributions. The CDF plots in particular show that for most values of ΔV^{th}, the two cost functionals would result in different decisions being made (with the ΔV cost resulting in the right one).

CONCLUSIONS

In summary, the theory of optimal control in conjunction with the Gauss pseudospectral method provides a robust framework for maneuver detection and validation in the context of UCT resolution. A key feature of the proposed method is the use of the total velocity increment ΔV as a cost function for evaluating the effort needed for a given maneuver. While alternate cost functions such as energy (2) can result in simpler control problems due to the absence of singularities in the objective function, a framework which uses ΔV is preferable because (i) the singularity issues can be resolved using the Huber approximation, (ii) it provides an accurate estimate of the ΔV effort and the correct optimal control when validated against analytically known solutions (whereas the minimum energy solution can overestimate the control effort significantly (by as much as 30% in our simulations)), and (iii) it produces a meaningful cost which can be compared to catalogs of ΔV data for known spacecraft. Further, the ΔV framework is robust and sufficiently general to accommodate the use of higher-order gravity models, non-conservative forces, and more general boundary conditions and path constraints.

We also demonstrated that the unscented transform and its higher-order versions provide an efficient way to approximate the first two moments of the control cost distribution in the case of uncertain boundary conditions, and a shifted Gamma distribution provides a good parametric fit to the actual PDF and CDF of the ΔV random variable. The method was found to be robust to a wide range of uncertainties in the boundary conditions. Finally, in a UCT association scenario considered, it was shown that using the actual ΔV cost functional in the optimal control problem, (i.e., solving an L_1 optimal control problem) is important for computing an accurate ΔV cost distribution, which in turn is critical in making the correct fuel-cost based UCT association decision.

ACKNOWLEDGMENTS

This work was funded by a Phase I SBIR from the Air Force Research Laboratory (AFRL), Rome NY (FA8750-11-C-0147), a Phase II SBIR from AFRL, Kirtland AFB (FA9453-11-C-0153), and a grant from the Air Force Office of Scientific Research (FA9550-11-1-0248). The authors also thank Dr. Marcus Holzinger and Dr. Scott Miller for useful discussions.

REFERENCES

[1] K. T. Alfriend, "A dynamic algorithm for the processing of UCTs," *AIAA/AAS Astrodynamics Conference 1997*, Sun Valley, ID, August 1997. Paper AAS-97-607.

[2] A. B. Poore, "Multidimensional assignment formulation of data association problems arising from multitarget tracking and multisensor data fusion," *Computational Optimization and Applications*, Vol. 3, 1994, pp. 27–57.

[3] M. J. Holzinger and D. J. Scheeres, "Object correlation, maneuver detection, and maneuver characterization using control effort metrics with uncertain boundary conditions and measurements," *AIAA Guidance, Navigation and Control Conference 2010*, Toronto, Canada, August 2010.

[4] Y. Bar-Shalom, X.-R. Li, and T. Kirubarajan, *Estimation with Applications to Tracking and Navigation*. New York: John Wiley & Sons, 2001.

[5] R. Hujsak and S. Reed, "A multiple models solution for real-time tracking of maneuvering satellites," White Paper, Analytical Graphics Inc., October 2008.

[6] I. Michael and Ross, "Space trajectory optimization and L1-optimal control problems," *Modern Astrodynamics* (P. Gurfil, ed.), Vol. 1 of *Elsevier Astrodynamics Series*, pp. 155 – VIII, Butterworth-Heinemann, 2007, 10.1016/S1874-9305(07)80008-2.

[7] P. J. Huber, "Robust regression: Asymptotics, conjectures and Monte Carlo," *Annals of Statistics*, Vol. 1, No. 5, 1973, pp. 799–821.

[8] D. F. Lawden, *Optimal Trajectories for Space Navigation*. Butterworths Mathematical Texts, London: Butterworths, 1963.

[9] S. J. Julier, J. K. Uhlmann, and H. F. Durant-Whyte, "A new method for the nonlinear transformation of means and covariances in filters and estimators," *IEEE Transactions on Automatic Control*, Vol. 55, 2000, pp. 477–482.

[10] A. E. Bryson and Y. Ho, *Applied Optimal Control*. Levittown, PA: Taylor & Francis, 1975.

[11] R. Fletcher, *Practical Methods of Optimization*. Chichester: John Wiley & Sons, 1991.

[12] D. A. Benson, G. T. Huntington, T. P. Thorvaldsen, and A. V. Rao, "Direct trajectory optimization and costate estimation via an orthogonal collocation method," *Journal of Guidance, Control, and Dynamics*, Vol. 29, No. 6, 2006, pp. 1435–1440.

[13] G. T. Huntington, *Advancement and Analysis of a Gauss Pseudospectral Transcription for Optimal Control Problems*. PhD thesis, Massachusetts Institute of Technology, 2007.

[14] D. A. Benson, *A Gauss Pseudospectral Transcription for Optimal Control*. PhD thesis, Massachusetts Institute of Technology, 2004.

[15] J. T. Horwood, N. D. Aragon, and A. B. Poore, "Covariance consistency for track initiation using Gauss-Hermite quadrature," *Proceedings of the 2010 Signal and Data Processing of Small Targets*, Orlando, FL, April 2010.

[16] S. J. Julier and J. K. Uhlmann, "Unscented filtering and nonlinear estimation," *Proceedings of the IEEE*, Vol. 92, 2004, pp. 401–422.

[17] G. H. Golub and J. H. Welsch, "Calculation of Gauss quadrature rules," *Mathematics of Computation*, Vol. 23, 1969, pp. 221–230, A1–A10.

[18] K. Ito and K. Xiong, "Gaussian filters for nonlinear filtering problems," *IEEE Transactions on Automatic Control*, Vol. 45, No. 5, 2000, pp. 910–927.

[19] A. Genz and B. D. Keister, "Fully symmetric interpolatory rules for multiple integrals over infinite regions with Gaussian weight," *Journal of Computational and Applied Mathematics*, Vol. 71, 1996, pp. 299–309.

[20] A. V. Rao, D. A. Benson, C. Darby, M. A. Patterson, C. Francolin, I. Sanders, and G. T. Huntington, "Algorithm 902: GPOPS, A MATLAB software for solving multiple-phase optimal control problems using the Gauss pseudospectral method," *ACM Transactions on Mathematical Software*, Vol. 37, April 2010, pp. 22:1–22:39, http://doi.acm.org/10.1145/1731022.1731032.

[21] P. E. Gill, W. Murray, and M. A. Saunders, "SNOPT: An SQP algorithm for large-scale constrained optimization," *SIAM Review*, Vol. 47, No. 1, 2005, pp. 99–131.

[22] D. A. Vallado, *Fundamentals of Astrodynamics and Applications*. New York: Springer, 2007.